Dual-frequency wavelength-tunable blue–green laser system for undersea applications

Hui Kong(孔辉)[1,2,4,†], Enlong Wang(王恩龙)[1,2,4,†,‡] Dongbo Lv(吕东博)[1,2], Peng Xie(谢鹏)[1,2], Haiping Xu(徐海萍)[1,2], Yuntao Xie(谢运涛)[1,2], Jintian Bian(卞进田)[1,2,3,§], Qing Ye(叶庆)[1,2], and Kejun Wang(王柯君)[1,2]

[1] *State Key Laboratory of Pulsed Power Laser Technology, National University of Defense Technology (NUDT), Hefei* 230037, *China*
[2] *Advanced Laser Technology Laboratory of Anhui Province, Hefei* 230037, *China*
[3] *Nanhu Laser Laboratory, National University of Defense Technology, Changsha* 410073, *China*

(Received 24 September 2025; revised manuscript received 23 October 2025; accepted manuscript online 15 December 2025)

A dual-frequency, wavelength-tunable blue–green laser system is demonstrated. The system utilizes a high-energy 532-nm green laser to pump a $KTiOPO_4$ (67.8°, 0°) optical parametric oscillator followed by a LiB_3O_5 (90°, 22.5°) second harmonic generator, generating blue laser light tunable from 447.6 nm to 459.7 nm with an overall frequency conversion efficiency of 4.2%. Both the residual green laser and the tunable blue laser can be emitted simultaneously, with energies of 11.24 mJ and 0.92 mJ, respectively. The beam quality factors M^2 of the green and blue lasers are $M^2(x,y) = (18.7, 12.6)$ and $M^2(x,y) = (29.5, 11.0)$, respectively, with corresponding energy stabilities of 6.1% and 13.9%. The blue laser pulse width is 6.84 ns, yielding a peak power of 134 kW. This laser system offers potential for various undersea applications where adaptable wavelength tuning is essential.

Keywords: blue–green laser, wavelength-tunable, undersea application

PACS: 42.60.By, 42.60.Jf, 42.62.–b

DOI: 10.1088/1674-1056/ae2c69 **CSTR:** 32038.14.CPB.ae2c69

1. Introduction

The blue–green spectral band serves as a transmission window for underwater propagation, facilitating underwater optical communication,[1] target detection,[2] marine resource exploration,[3] and geological risk prediction.[4] Studies have demonstrated that green lasers within a range of 520 nm–550 nm offer higher transmission in coastal seawater, whereas blue lasers in a range of 450 nm–490 nm exhibit better performance in deep seawater.[5] Notably, Fraunhofer lines at 486.134 nm (H-β) and 527.039 nm (Mg) coincide with solar absorption bands, rendering these wavelengths less affected by sunlight background noise. Consequently, blue/green lasers at these specific wavelengths have attracted extensive research interest.[5,6] Consider a scenario involving autonomous underwater vehicles (AUVs)[7] that adapt to gradual changes in seawater quality during diving and exploration. In such cases, it is preferable for the laser source to offer multiple or tunable wavelengths to accommodate varying marine conditions and maximize transmission distance. Although dual- or multi-wavelength blue–green lasers[3,8] provide certain advantages, they increase system cost and still limit the wavelength tuning range. Therefore, lasers with broader wavelength tunability are more desirable to enhance adaptability. Consequently, there is an urgent demand for high-power, wavelength-tunable blue–green lasers to support various undersea applications.

Existing methods for direct blue light generation — including LEDs,[1] gas lasers,[9] and nitride semiconductor devices (GaN/InGaN)[10–12] — have limited peak output energy and restricted wavelength tuning ranges. Solid-state approaches play a crucial role in producing high-power, wavelength-tunable blue lasers, primarily through nonlinear frequency conversion of near-infrared lasers. Among these, harmonic generation is widely employed for high-power blue-band emission. For example, frequency doubling of the 946-nm, 914-nm, and 912-nm transitions of Nd^{3+} yields 473-nm,[13] 457-nm,[14] and 456-nm[15] radiation, respectively. Third-harmonic generation of the 1319-nm Nd^{3+} line produces 440 nm,[16] while fourth-harmonic conversion of the 1946-nm Tm^{3+} transition delivers 486 nm.[17] However, these quasi-three-level pump schemes generally exhibit moderate quantum efficiency and require additional suppression of parasitic lines; moreover, continuous wavelength tuning remains challenging.

Optical parametric oscillation (OPO) is a crucial frequency conversion technique in solid-state lasers, enabling widely tunable wavelengths and high peak power. Tunable blue sources based on solid-state lasers have been investigated by several research groups. For instance, Lu *et al.* proposed

[†]These authors contributed equally to this work.
[‡]Corresponding author. E-mail: wangenlong15@nudt.edu.cn
[§]Corresponding author. E-mail: bianjt@126.com

© 2026 Chinese Physical Society and IOP Publishing Ltd. All rights, including for text and data mining, AI training, and similar technologies, are reserved.

CPB Online In-Press

sum-frequency mixing between a 1-μm fundamental beam and the signal wave of a 0.9-μm OPO to extend tunability into the blue region.[18] Zhang *et al*. demonstrated a compact, wavelength-tunable pulsed laser output around 440 nm with a 27-nm tuning range for oceanic lidar applications.[19] Wu *et al*. pumped a $KTiOPO_4$ (KTP) OPO with 532-nm light to generate 886-nm signal radiation, which was then frequency-doubled to 443 nm in an LiB_3O_5 (LBO) crystal;[20] however, wavelength tuning was not implemented.

It should be noted that frequency conversion based on novel laser types has also demonstrated promising performance in blue laser generation. For example, Deng *et al*. employed frequency tripling of a 1412 nm–1435.5 nm Raman random fiber laser to generate blue light within the range of 470.6 nm–478.7 nm; however, the optical-to-optical efficiency is limited to only 0.1%.[21] Peng *et al*. demonstrated a high-power, frequency-doubled 490-nm blue laser from a semiconductor disk laser, achieving a wavelength tuning range of 21.5 nm;[22] nevertheless, it requires a specifically designed gain chip, which increases complexity and costs. Table 1 summarizes the current methods for extending the wavelength span of blue–green lasers in undersea applications.

To achieve simultaneous high power and wavelength tunability in blue–green lasers, this article presents an alternative frequency conversion approach by combining OPO and SHG in series. The current configuration employs 532-nm light to pump a KTP crystal, generating tunable 904-nm radiation that is subsequently frequency-doubled in an LBO crystal. Both crystals utilize angle tuning to extend the wavelength tuning range, producing continuously tunable blue light centered at 452 nm. This design addresses the previously unexplored 452-nm wavelength band while maintaining a compact architecture. Additionally, the residual 532-nm green light and the generated tunable 452-nm blue light can be simultaneously output, making the system well-suited for implementation on AUVs and offering potential applications in various undersea operations.

Table 1. Solutions for extending the wavelength span of blue–green lasers for undersea applications. SSL: solid state laser; DP-SSL: diode pumped SSL; SDL: semiconductor disk laser; RFL: Raman fiber laser.

Solution	Source type	Wavelength (nm)	Power/Energy	Ref.
Dual wavelength	SSL	532, 480	10.6 mJ, 9.6 mJ	Ma (2022)[3]
	SSL	532, 355	200 mJ, 120 mJ	Liu (2022)[4]
	DP-SSL	532, 491	50 mW, 50 mW	Zhang (2023)[8]
Tunable wavelength	SSL	432.2–459.1	1.32 mJ	Zhang (2021)[19]
	SSL	443	4.08 mJ	Wu (2025)[20]
	RFL	470.6–478.7	0.1 mW	Deng (2025)[21]
	SDL	480–500	5.36 W	Peng (2024)[22]
Dual + tunable	SSL	532, 447.6–459.7	11.24 mJ, 0.92 mJ	This work

2. Methods

2.1. Experimental setup

The experimental setup for blue–green laser generation and its potential application in a water tank experiment is illustrated in Fig. 1. It comprises an OPO conversion stage using a KTP crystal, which upconverts the 532-nm green laser pump to 904 nm, followed by an SHG stage with an LBO crystal that frequency-doubles the 904-nm radiation to 452 nm. The 532-nm laser source (model LS-607A) delivers a collimated beam with a 6-mm diameter, a repetition rate continuously adjustable from 1 Hz to 10 Hz, and pulse energy ranging from 2 mJ to 50 mJ. The pulse duration is approximately 8 ns. Mirror F1 is anti-reflection coated for 532 nm (transmission $T > 99\%$) and high-reflection coated for 1064 nm (reflectivity $R > 95\%$), ensuring that only the 532-nm radiation enters the OPO cavity.

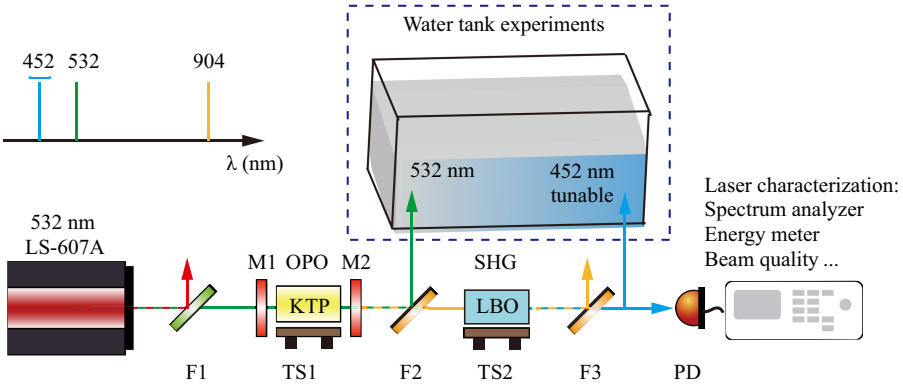


Fig. 1. Schematic diagram of the experimental setup, see text for more details. KTP: $KTiOPO_4$ crystal; LBO: LiB_3O_5 crystal; OPO: optical parametric oscillation; SHG: second harmonic generation; TS: translation stage; PD: photodetector.

CPB Online In-Press

The OPO cavity, comprising mirrors M1 and M2 together with the KTP crystal, is configured for collinear pumping. Both M1 and M2 have identical coatings: high transmission at 532 nm and 900 nm–910 nm ($T > 99\%$), and high reflection at 1280 nm–1300 nm ($R > 95\%$). The KTP crystal is cut at $\theta = 67.8°$ and $\phi = 0°$, with clear-aperture dimensions of 10 mm × 10 mm × 25 mm (25 mm along the propagation axis). It is mounted in a 3D-printed annular holder fixed on a compact Zolix NVM25.4 precision translation stage (TS1) with short transverse dimensions. This mechanical design reduces the OPO resonator length to 35 mm, enhancing the optical-to-optical conversion efficiency. Mirror F2 is high-reflection coated for 532 nm ($R > 99\%$), which rejects residual pump radiation while transmitting the generated 904-nm signal light directed into the LBO crystal.

The LBO crystal is cut for type-I phase matching at $\theta = 90°$ and $\phi = 22.5°$, with dimensions of 8 mm × 8 mm × 12 mm (12 mm along the optical path). Mirror F3 is high-reflection coated for 900 nm–910 nm ($R > 98\%$) and high-transmission coated for 400 nm–500 nm ($T > 92\%$), allowing the generated blue radiation to reach the energy meters unobstructed.

Output pulse energies are measured using a laser radiometer (Probe F40J-SM) for high energy and a Thorlabs energy meter (Probe ES111C) for lower energy. The spectral characteristics of the 904-nm and 452-nm lasers are recorded with a near-infrared spectrometer (Aurora 4000, 200 nm–1100 nm). Pulse durations are determined using a DH-GDT-D103VB photodetector and a Keysight DSO3024T oscilloscope. Future water tank experiments are planned.

2.2. Theoretical calculations

The wavelength tuning of the blue laser relies primarily on the angle phase-matching of the KTP OPO. In addition, a dedicated angle adjustment of the LBO crystal is used to maintain optimal SHG efficiency across the tuning range.

In the first stage, an OPO employing a KTP crystal under type II-B phase matching is utilized to generate a 904-nm laser. This specific configuration requires the satisfaction of the following phase-matching condition, which ensures the conservation of energy and momentum:

$$\frac{1}{\lambda_3} = \frac{1}{\lambda_1} + \frac{1}{\lambda_2}, \tag{1}$$

$$\frac{n_{e_2}^{\lambda_3}}{\lambda_3} = \frac{n_{e_1}^{\lambda_1}}{\lambda_1} + \frac{n_{e_2}^{\lambda_2}}{\lambda_2} \quad \text{(type II-B)}, \tag{2}$$

where λ_1, λ_2, and λ_3 are the wavelengths of the signal, idler, and pump waves, respectively. $n_{e_2}^{\lambda_3}$ denotes the refractive index of fast light at λ_3; $n_{e_1}^{\lambda_i}$ and $n_{e_2}^{\lambda_i}$ denote the refractive indices of slow light and fast light at λ_i ($i = 1, 2$). These indices are functions of the propagation direction (θ, ϕ) within the crystal and are given by the Sellmeier equations.[23] Figure 2(a) shows the calculated type II-B phase-matching tuning curve for KTP with $\phi = 0°$ under 532-nm pump. The signal and idler wavelengths are depicted by the red and blue solid lines, respectively, as functions of the internal angle θ. Based on this calculation, the KTP crystal was cut at $(\theta, \phi) = (66.5°, 0°)$ to fulfill the phase-matching condition. The experimental data for the 904-nm wavelength, marked by red circles in Fig. 2(a), are in excellent agreement with the calculation.

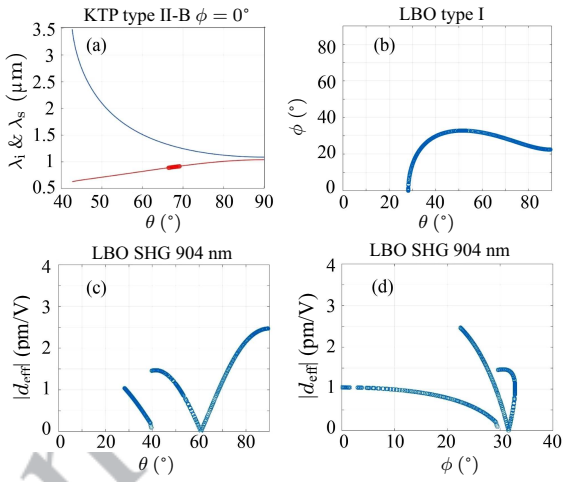


Fig. 2. Theoretical calculations: (a) output wavelength of KTP OPO under type II-B phase matching with $\phi = 0°$; (b) LBO SHG phase matching curve under type I condition; (c) and (d) the effective nonlinear coefficient of LBO SHG with 904-nm incident light for θ and ϕ angles, respectively.

In the second stage, the 904-nm laser is frequency-doubled to 452 nm using an LBO crystal in a type-I phase-matching configuration. This process must also satisfy the fundamental energy conservation (Eq. (1)) and momentum conservation relations:

$$\frac{n_{e_2}^{\lambda_3}}{\lambda_3} = \frac{n_{e_1}^{\lambda_1}}{\lambda_1} + \frac{n_{e_1}^{\lambda_2}}{\lambda_2} \quad \text{(type I)}. \tag{3}$$

In the SHG case, the signal (λ_1) and idler (λ_2) waves are degenerate. For a given propagation direction inside the birefringent LBO crystal, defined by the angles (θ, ϕ), a continuum of solutions satisfies the phase-matching condition, as illustrated in Fig. 2(b). However, the conversion efficiency depends strongly on the effective nonlinear coefficient d_{eff}, which varies with the crystal orientation angles (θ, ϕ).[24,25] This coefficient is derived from the second-order nonlinear susceptibility tensor d_{ijk} of LBO and the polarization vectors of the interacting waves.[26] It is expressed as

$$d_{\text{eff}} = \sum_{i,j,k=X,Y,Z} (\hat{e}_{2\omega})_i \cdot d_{ijk} \cdot (\hat{e}_{\omega})_j \cdot (\hat{e}_{\omega})_k, \tag{4}$$

where $\hat{e}_{\omega}$ and $\hat{e}_{2\omega}$ are the unit polarization vectors of the fundamental (904 nm) and second harmonic (452 nm) waves, respectively. This expression represents a summation over the relevant tensor components d_{ijk} projected onto these polarization directions.

To maximize the output energy at 452 nm, we selected phase-matching angles (θ, ϕ) corresponding to a high effective nonlinear coefficient d_{eff}. Based on the known d-tensor

CPB Online

of LBO,[26] Figs. 2(c) and 2(d) show the calculated variation of d_{eff} with θ and ϕ, respectively, providing guidance for the optimal crystal angle selection. As shown in Figs. 2(c) and 2(d), the effective nonlinear coefficients reach their maximum value of approximately 2.47 pm/V at $\theta = 89.4°$ and $\phi = 22.5°$, respectively. To simplify fabrication, the LBO crystal was custom-cut with orientation angles (90°, 22.5°), aligning with the principal axes while maintaining near-optimal performance. Furthermore, a crystal optical path length of 12 mm was chosen to ensure high conversion efficiency.

3. Results and analysis

A series of characterizations of the blue–green laser system were performed, demonstrating the feasibility of generating blue light with a tunable wavelength range from 447.6 nm to 459.7 nm, exhibiting a linear energy scaling relationship, moderate beam quality, and energy stability.

3.1. Spectra and energy scaling

Under normal incidence, the KTP OPO outputs a 904-nm laser, which is frequency-doubled to generate a 452-nm laser through the LBO crystal. When mirror F3 is removed, the Aurora 400 near-infrared spectrometer can simultaneously measure the spectra of the 532-nm, 904-nm, and 452-nm lasers, as shown in Fig. 3(a).

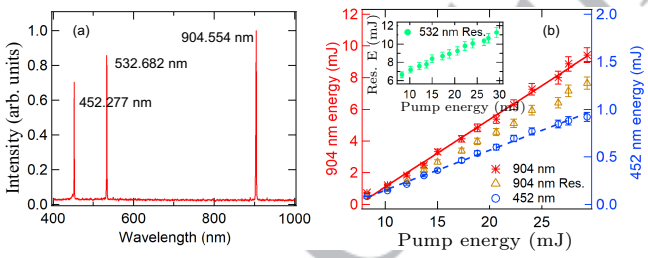


Fig. 3. (a) Output spectra of the 532-nm, 904-nm, and 452-nm lasers; (b) energy scaling of the 904-nm and 452-nm outputs *versus* the 532-nm pump energy, orange triangles represent the residual 904-nm pulse energy. Inset shows the residual 532-nm green pulse energy as a function of the pump energy.

The energy scaling relationships of the 904-nm and 452-nm laser pulses as a function of the 532-nm pump energy are characterized, as shown in Fig. 3(b). By positioning an energy meter at the transmission of mirrors F2 and F3, the pulse energies of the 904-nm and 452-nm lasers can be measured. The red stars in Fig. 3(b) represent the measured values of the 904-nm laser, corresponding to the left vertical axis, while the blue circles represent the measured values of the 452-nm laser, corresponding to the right vertical axis. When the pump laser energy at 532 nm increases from 8.25 mJ to 29.35 mJ, the energy of the 904-nm signal generated by the KTP OPO increases from 0.73 mJ to 9.42 mJ. After passing through the LBO crystal, the 904-nm laser undergoes frequency doubling to produce the 452-nm laser, with its energy increasing from 85 μJ to 0.92 mJ. The residual 904-nm pulse energy, measured at the reflection of mirror F3, is represented by the orange triangles referenced to the left vertical axis. Based on linear fits to the measured output energies at 904 nm and 452 nm versus the 532-nm pump energy, the optical-to-optical conversion efficiencies of the OPO and SHG stages are calculated to be 42.6% and 9.8%, respectively, corresponding to an overall efficiency of 4.2% for the conversion from 532-nm pump to blue laser emission at 452 nm.

The residual energy of the 532-nm pump pulses is measured using an energy meter placed at the reflection of mirror F2. As shown in the inset of Fig. 3(b), the residual pump energy reaches 11.24 mJ at the maximum pump energy of 29.35 mJ. This green pulse can be output simultaneously with the generated 452-nm blue pulse, making the source suitable for underwater detection applications.

3.2. Wavelength tuning of the blue laser

Wavelength tuning of the blue laser primarily relies on the OPO stage, where angle tuning of the KTP crystal is achieved using the Zolix NVM25.4 translation stage (TS1). When the screw of TS1 is rotated one full turn, the external incident angle θ on the crystal changes by approximately 0.243°. Considering that the refractive index of the KTP crystal is approximately 1.7892, the internal incident angle θ' changes by about 0.136°. As the crystal angle is tuned from 66.4° to 69.2°, the output wavelength shifts from 889.0 nm to 916.2 nm, which agrees well with theoretical predictions, as shown in Fig. 2(a).

The generated tunable 904-nm laser subsequently passes through the LBO crystal, where second harmonic generation occurs. The LBO crystal oriented at (90°, 22.5°) enables frequency doubling of the 904-nm laser to 452 nm and possesses a specific allowable linewidth. When the laser wavelength generated by the KTP OPO deviates beyond this allowable linewidth from the 904-nm central wavelength, efficient frequency doubling cannot be achieved. To extend the wavelength tuning range of the blue laser, the LBO crystal is also mounted on a translation stage (TS2), which enables angle tuning to optimize conversion efficiency. TS2 provides the same tuning resolution as TS1 and adjusts the ϕ angle of the LBO crystal around a center value of 22.5°. Given that the refractive index of LBO at 904 nm is approximately 1.568, one full rotation of the tuning screw corresponds to an internal angle change of about 0.155°.

By combining the angular adjustments of both TS1 and TS2, the overall tuning range of the blue laser wavelength can be extended. Experimentally, blue laser emission around 452 nm was achieved over a wavelength range of 447.6 nm–459.7 nm, as shown in Fig. 4. It should be noted that the optimal LBO angle varies with the wavelength of the pump laser, consistent with the theoretical calculations from Subsection 2.2. The current wavelength tuning range of the 452-nm blue laser is limited by the angular tuning range of the OPO

CPB Online In-Press

crystal, though it can theoretically be extended up to the acceptance bandwidth of the LBO crystal.

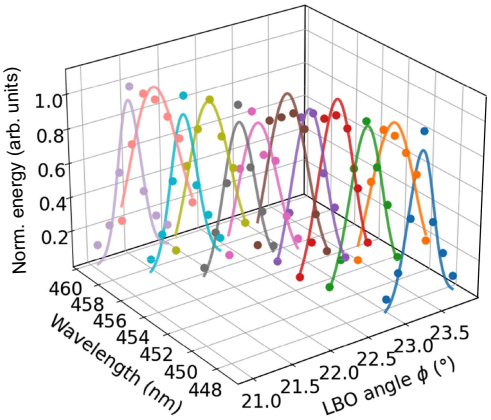


Fig. 4. Wavelength tuning of the blue laser by changing the angles of the KTP and LBO crystals.

3.3. Beam profile and quality

The beam profile and the M^2 quality factor of the 532-nm and 452-nm blue laser pulses are measured using a beam quality analyzer (CinCam CCD-2302). For the high-energy 532-nm green pump, the beam was first split by a polarizing beam splitter (PBS) and then focused using an $f = 100$ mm lens. It was subsequently attenuated by 20 dB before incidence on the CCD camera. The beam radii in the x- and y-directions are extracted from a Gaussian fit of the beam profile, yielding the $1/e^2$ radii w_x and w_y, as shown in the inset of Fig. 5(a). The distance between the lens and the camera ranges from 65 mm to 210 mm, and the beam radii are measured at different positions, as illustrated in Fig. 5(a).

The evolution of the beam radius ($w_{(z)}$) in the x- and y-directions as a function of the propagation distance (z) is fitted with the following function

$$w_{(z)} = w_0\sqrt{1+\left(\frac{z-z_0}{z_R}\right)^2}, \tag{5}$$

where w_0 is the beam waist radius, z_0 denotes the waist location, and z_R represents the Rayleigh range. The M^2 beam quality factor, which quantifies the deviation from an ideal Gaussian beam, is calculated from the fitted parameters of Eq. (5) as

$$M^2 = \frac{\pi w_0^2}{\lambda z_R}, \tag{6}$$

where $\lambda = 532$ nm is the wavelength. Based on this analysis, the beam quality factors for the 532-nm green pulse are determined to be $M_x^2 = 18.7$ and $M_y^2 = 12.6$, respectively.

For the blue pulse at 452 nm, the output pulse is focused with an $f = 100$ mm lens and attenuated by 20 dB before being incident on the camera. The beam profile exhibits an elliptical shape with an aspect ratio of approximately 1.2, as shown in the inset of Fig. 5(b). The beam quality factors of the 452-nm blue pulse are determined to be $M_x^2 = 29.5$ and $M_y^2 = 11.0$, respectively. Judging from the M^2 factors, both the green and blue pulses exhibit relatively poor beam quality;[27] notably, the quality of the generated 452-nm beam is degraded compared to that of the 532-nm pump source. The degradation in beam quality is primarily caused by spatial walk-off in the LBO crystal.[28] This nonlinear effect occurs because the birefringent crystal is cut at a specific angle, causing the ordinary and extraordinary waves to separate spatially as they propagate, which distorts the beam. To mitigate this, one can employ a pair of reversely-oriented LBO crystals to cancel out the walk-off or use temperature tuning to achieve non-critical phase matching, which eliminates walk-off entirely.[29]

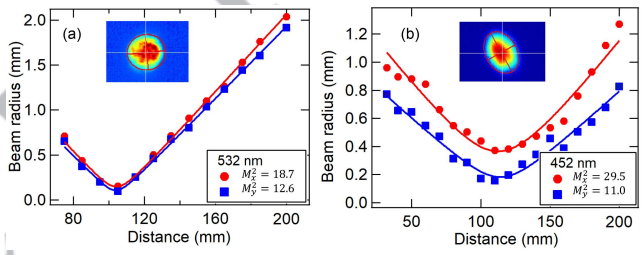


Fig. 5. Beam quality and M^2 factor of the 532-nm (a) and 452-nm (b) laser beams. Insets show typical images of the beam profile.

3.4. Pulse width and energy stability

When the angle θ of the KTP crystal is 67.8° (under normal incidence), the pulse widths (full width at half maximum, FWHM) of the lasers before and after the OPO and SHG conversion processes are measured. Typical results are shown in Fig. 6(a). The pulse widths of the lasers at 532 nm, 904 nm, and 452 nm are 7.305 ns, 4.486 ns, and 6.840 ns, respectively. During the conversion of the 532-nm laser to the 904-nm laser, the signal light oscillates within the OPO cavity, achieving an optical-to-optical conversion efficiency of approximately 42.6%. Partial inverse conversion occurs at the pulse peak, resulting in pulse narrowing. In the subsequent conversion from the 904-nm laser to the 452-nm laser, the beam passes once through the LBO crystal, with an optical-to-optical conversion efficiency of about 9.8%. Only the region near the pulse peak participates in the conversion, causing pulse broadening. The peak power of the blue laser is calculated as 134 kW, considering a peak energy of 0.92 mJ.

The laser pulse energy stability is evaluated by recording the energy over 1000 consecutive pulses at a repetition rate of 1 Hz using a Thorlabs energy meter (Probe ES111C). To prevent detector damage and accommodate the limited measurement range of the energy sensor, the residual 532-nm pulse was split, with only a fraction directed onto the energy probe.

CPB Online Press

This energy splitting does not affect the relative pulse-to-pulse stability. The results are shown in Fig. 6(c), where green squares and blue circles represent the 532 nm and 452-nm pulses, respectively. Figures 6(b) and 6(d) display the corresponding statistical distributions, both of which follow a normal distribution. Gaussian fitting yields relative energy instabilities of 6.1% for the 532-nm pulses and 13.9% for the 452-nm pulses. The higher instability observed in the 452-nm output compared to the 532-nm pump can be attributed to temperature fluctuations during the nonlinear conversion process. Implementing active temperature control for the KTP and LBO crystals could further reduce this instability.[30]

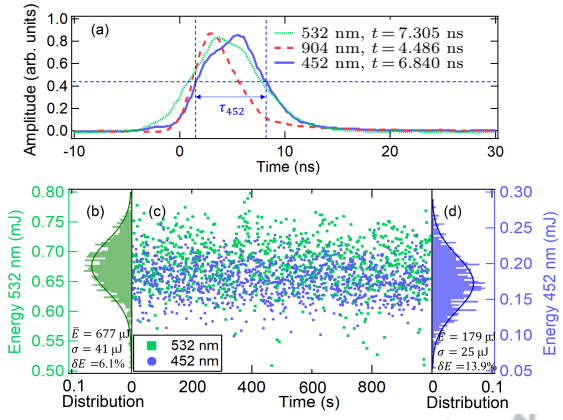


Fig. 6. (a) Pulse widths of the 452-nm, 904-nm, and 532-nm lasers, respectively; (c) energy instability of the 532-nm and 452-nm pulses over 1000 consecutive measurements; (b) and (d) Gaussian fits of the energy data showing normal distributions for the 532-nm and 452-nm pulses, respectively.

4. Conclusion

A tunable blue laser covering the wavelength range of 447.6 nm–459.7 nm with a peak power of up to 134 kW is demonstrated for the first time, to the best of our knowledge. Combined with the residual 532-nm green pump, the system can simultaneously output green and tunable blue laser pulses, making it suitable for undersea laser detection missions under varying water quality and depth conditions. In the future, employing frequency-doubling crystals with higher allowable linewidth could enable a blue laser with an extended tuning range. The blue laser energy can be further increased by raising the pump energy and through other optimization methods. Based on the damage threshold of the LBO crystals, the blue laser output energy is estimated to reach the order of 10 mJ, with a peak power between 1 MW and 10 MW. This laser system can be directly applied in water tank experiments to measure beam transmission loss and has potential for integration into various autonomous underwater vehicles.

Acknowledgement

Project supported by the Independent Innovation Science Foundation of NUDT (Grant Nos. 23-ZZCX-JDZ-44 and ZK23-47).

References

[1] Wu T C, Chi Y C, Wang H Y, Tsai C T and Lin G R 2017 *Sci. Rep.* **7** 40480
[2] Chen Y Q, Luo Q H, Guo S C, Chen W B, Hu S J, Ma J, He Y and Huang Y F 2024 *Opt. Commun.* **551** 129903
[3] Ma J, Lu T T, He Y, Jiang Z Y, Hou C H, Li K P, Liu F H, Zhu X L and Chen W B 2020 *Appl. Opt.* **59** C87
[4] Liu Q, Wu S H, Liu B Y, Liu J T, Zhang K L, Dai J Y, Tang J W and Chen G 2022 *Opt. Express* **30** 8927
[5] Zhang J X, Ma J, Lu T T, Zhu X L, He Y and Chen W B 2025 *Appl. Opt.* **64** 4341
[6] Luo Q H, Ma J, Huang Z Z, Lu T T, Zhang J X, Ma H D, Zhu X L and Chen W B 2025 *Appl. Phys. B* **131** 1
[7] Zhang K X, Li Z, Wang Z X, Wang K Q and Ma X X 2023 *Semiconductor Lasers and Applications XIII* **12761** 147
[8] Zhang H W, He Y, Li Z W, Chen X C, Dai G Y, Yin B, Tang J W, Chen W B and Wu S H 2023 *Opt. Express* **31** 12311
[9] Golombek A, Breuer L, Danzig L, Kucharczyk P, Schleberger M, Sokolowski-Tinten K and Wucher A 2021 *New J. Phys.* **23** 033023
[10] Eliwa M N, Alatawi A A, Holguín-Lerma J A, Alkhazragi O, Ashry I, Ng T K and Ooi B S 2021 *IEEE Photonics J.* **13** 1
[11] Verma G, Wang E L, Assendelft J, Poli N, Rosi G, Tino G M and Salvi L 2022 *Appl. Phys. B* **128** 100
[12] Qin F F, Sun Y, Yang Y, Li X, Wang X, Lu J F, Wang Y J and Zhu G Y 2023 *Chin. Phys. B* **32** 054210
[13] Chen F, Yu X, Guo J, Guo L H, Yang G L, Xie J J, Zhang L M, Geng Y M, Li S M, Li D J, Shao C L, Meng F J, Zhang C S and Yan R P 2012 *Laser Phys.* **22** 81
[14] Gao J, Yu X, Li X D, Chen F, Zhang Z, Yu J H and Wang Y Z 2008 *Laser Phys. Lett.* **5** 433
[15] Chen F, Yu X, Zhang K, He Y, Zheng C B, Wang C R and Guo J 2015 *Opt. Laser Technol.* **68** 36
[16] Mu X D and Ding Y J 2005 *Opt. Lett.* **30** 1372
[17] Creeden D, Blanchard J, Pretorius H, Limongelli J and Setzler S D 2016 *Fiber Lasers XIII: Technology, Systems, and Applications* **9728** 400
[18] Lu T T, Ma J, Zhu X L and Chen W B 2019 *Chin. Opt. Lett.* **17** 051405
[19] Zhang J L, Ma J, Lu T T, Liu D, Zhu X L and Chen W B 2021 *Opt. Commun.* **485** 126706
[20] Wu H D, Chen F T, Yuan M Z, Dong J Y, Sun W B, Hu M, Liu D and Liu C 2025 *Appl. Opt.* **64** 808
[21] Deng W, Chen L, Bo Z W, Fan M Q, Leng Z T, Liang H K, Hu B and Wu H 2025 *Opt. Lett.* **50** 2045
[22] Peng X F, Wang T, Zhu R J, Jiang L D, Tong C Z, Song Y R and Zhang P 2024 *Opt. Express* **32** 36535
[23] Kong H, Bian J T and Sun X Q 2019 *Optik* **193** 163004
[24] Kong H, Bian J T, Yao J Y, Ye Q and Sun X Q 2021 *Chin. Opt. Lett.* **19** 021901
[25] Bian J T, Kong H, Ye Q, Yao J Y, Guo L and Sun X Q 2022 *Chin. Opt. Lett.* **20** 041901
[26] Yao J Q, Sheng W D and Shi W Q 1992 *J. Opt. Soc. Am. B* **9** 89
[27] Liu Y, Li Z Y, Yao J Y, Wang H, Zhu Z R, Bai J Z, Fu J J, Lu Y, Zheng Y J and Tan R Q 2024 *Opt. Lett.* **49** 3255
[28] Ohae C, Hasegawa K, Nagano M, Tahara S and Katsuragawa M 2023 *Opt. Express* **31** 41471
[29] Liu B Z, Li X Y, Dong J H, Zhang L and Li L J 2025 *Chin. Phys. B* **34** 094208
[30] Wang K J, Kong H, Li X X, Lv D B and Xie P 2025 *Chin. Phys. B* **35** 014210

CPB Online In Press